

## THE EXACT SEISMIC RESPONSE OF AN OCEAN AND A N-LAYER CONFIGURATION\*

G.G. DRIJKONINGEN\*\* and J.T. FOKKEMA\*\*\*

### ABSTRACT

DRIJKONINGEN, G.G. and FOKKEMA, J.T. 1987, The Exact Seismic Response of an Ocean and a N-Layer Configuration, *Geophysical Prospecting* 35, 33-61.

The space-time acoustic wave motion generated by an impulsive monopole source is calculated with the aid of the Cagniard-de Hoop technique. Two configurations with plane interfaces are discussed: an air/fluid/solid configuration with the source and the receiver located in the fluid layer; and a stack of  $n$  fluid layers between two acoustic half-spaces where the source and the receiver are located in the upper half-space. Synthetic seismograms are generated for the pressure of the reflected wavefield, using the source signature of an airgun.

### INTRODUCTION

The acoustic wavemotion for two different configurations is analyzed. In one configuration a fluid layer is bounded on the upper side by a half-space of air, while the lower half-space is filled with an isotropic, perfectly elastic material. In this configuration an impulsive monopole point source or line source is located in the fluid. The receiver is positioned in the fluid layer. The second configuration consists of a stack of fluid layers bounded on both sides by an acoustic half-space, where the source and receiver are located in the upper half-space (Aki and Richards 1980). The acoustic response to the source excitation has been calculated by the Cagniard-de Hoop technique.

The Cagniard-de Hoop technique, introduced by Helmberger (1968), is now well established in pure seismology. The mathematical foundations were developed by Cagniard (1939, 1962) and de Hoop (1960). (The latter gives a clear discussion of the technique.) Its application to seismic prospecting, however, has not been so common although the technique is highly valuable for forward modeling since it gives the

\* First part read at the 47th meeting of the EAEG, Budapest, June 1985, last material received May 1986.

\*\* Department of Earth Sciences, Bullard Laboratories, Madingley Rise, Madingley Road, Cambridge CB3 0EZ, UK.

\*\*\* Delft University of Technology, Department of Mining Engineering, Section Technical Geophysics, POB 5028, 2600 GA Delft, The Netherlands.

exact solution. Here the exact solutions are evaluated but faster programs, with about the same accuracy, could be achieved by introducing high-frequency approximations (see Helmberger 1968).

In the three-layer problem the two boundaries together are the cause of multiply reflected waves. In a stack of fluid layers only the primary reflections are considered, thus no internal multiply reflected waves will be involved. To apply the Cagniard-de Hoop technique, we assumed the fluids to be homogeneous, ideal and lossless and the solid, if present, to be isotropic, homogeneous and perfectly elastic.

We begin our analysis by presenting the general framework. Then we discuss the two configurations separately, the first more extensively. We introduce the fundamental wavemotion in the media on which our model depends. The different wavefields are connected by the boundary conditions for the media, which leads to a final wavefield representation. With this method Green's function in the space-time domain is determined. The two-dimensional case (the line source problem) and the three-dimensional case (the point source problem) are presented. Firstly the space-time Green's function is computed and then convolution with a known source signature is performed.

## PART 1. AIR/FLUID/SOLID CONFIGURATION WITH THE SOURCE AND RECEIVER IN THE FLUID

### 1.1. General framework

To specify space and time  $x$ ,  $y$  and  $z$  are the spatial coordinates and  $t$  the time coordinate. We chose a right-handed Cartesian coordinate system with the  $z$ -axis pointing downwards and the  $x$ - $y$  plane forming the interface between the air and fluid layers (fig. 1). Both the source and receiver are positioned in the fluid. The source and receiver depths are denoted by  $h_s$  and  $h_r$ , respectively, while the layer thickness is given by  $h_w$ . The quantities which describe the properties of the media

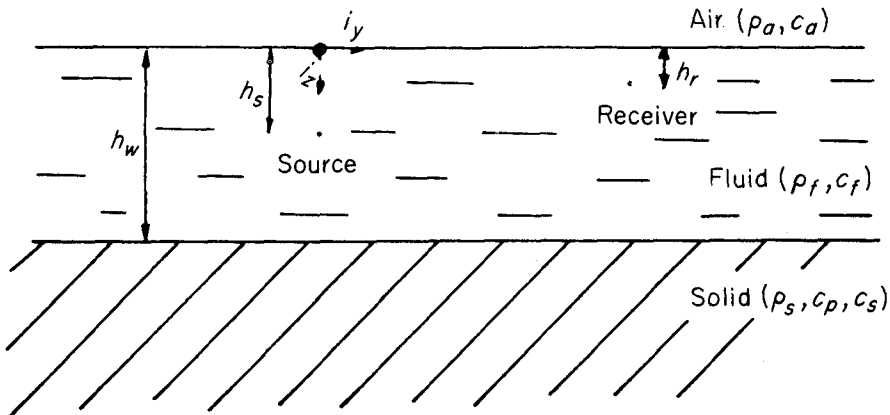


Fig. 1. The first configuration to be considered.

Table 1. *Quantity description.*

Quantity	Description	SI-units
$\rho_a, \rho_f, \rho_s$	volume density of mass ( $a = \text{air}, f = \text{fluid}, s = \text{solid}$ )	$\text{kg/m}^3$
$K_a, K_f$	bulk modulus of compression ( $a = \text{air}, f = \text{fluid}$ )	$\text{N/m}^2$
$\lambda, \mu$	Lamé coefficients	$\text{N/m}^2$
$c_a = (K_a/\rho_a)^{1/2}$	wave velocity in air	$\text{m/s}^2$
$c_f = (K_f/\rho_f)^{1/2}$	wave velocity in fluid	$\text{m/s}^2$
$c_p = ((\lambda + 2\mu)/\rho_s)^{1/2}$	compressional-wave velocity in solid	$\text{m/s}^2$
$c_s = (\mu/\rho_s)^{1/2}$	shear-wave velocity in solid	$\text{m/s}^2$

can be found in table 1. The fluid is assumed to be lossless, homogeneous and ideal, while the lower half-space is filled with an homogeneous, isotropic, perfectly elastic solid. The source starts to act at time  $+0$ . With these assumptions the equations can be transformed from time ( $t$ ) to Laplace domain ( $s$ ) where  $s$  is chosen positive real, and from  $x$  and  $y$  to the spatial Fourier domain ( $\alpha x, \beta y$ ) through

$$\hat{f}(x, y, z; s) = \int_{0-}^{\infty} f(x, y, z; t) \exp(-st) dt, \quad (1)$$

$$\tilde{f}(s\alpha, s\beta, z; s) = \iint_{-\infty}^{+\infty} \hat{f}(x, y, z; s) \exp\{js(\alpha x + \beta y)\} dx dy. \quad (2)$$

The transformation back to the space-Laplace domain is written as

$$\hat{f}(x, y, z; s) = \left(\frac{s}{2\pi}\right)^2 \iint_{-\infty}^{+\infty} \tilde{f}(s\alpha, s\beta, z; s) \exp\{-js(\alpha x + \beta y)\} d\alpha d\beta. \quad (3)$$

Note that a circumflex ( $\hat{\cdot}$ ) refers to a Laplace transformed quantity, while a tilde ( $\tilde{\cdot}$ ) denotes a Laplace-Fourier transformed quantity.

The total wavefield in the fluid is decomposed into an incident field and a reflected field (indicated by superscripts  $i$  and  $r$ ), where the incident field is the field which would be present if the fluid were of infinite extent, and the reflected field is the difference between the actual wavefield and the incident field.

Let  $p$  denote the pressure (Pa). We start with the inhomogeneous wave equation for the incident field,

$$\left(\partial_x^2 + \partial_y^2 + \partial_z^2 - \frac{1}{c_f^2} \partial_t^2\right) p^i = -\rho_f \partial_t^2 \varphi_v(t) \delta(x, y, z - h_s), \quad (4)$$

where

$$\varphi_v(t) = \text{volume density of injected fluid volume}, \quad (5)$$

and the partial derivative  $\partial_i^2$  is given by

$$\partial_i^2 = \frac{\partial^2}{\partial_i^2} \quad (i = x, y, z, t). \quad (6)$$

Then performing the Laplace and Fourier transformations,

$$d_z^2 \tilde{p}^i - s^2 \gamma_f \tilde{p}^i = -s^2 \rho_f \hat{\phi}_v \delta(z - h_s), \quad (7)$$

where

$$\gamma_f = (1/c_f^2 f + \alpha^2 + \beta^2)^{1/2} \quad \text{with } \text{Re}(\gamma_f) \geq 0. \quad (8)$$

The solution of this inhomogeneous differential equation is well known:

$$\tilde{p}^i = A^i \exp(-s\gamma_f |z - h_s|), \quad (9)$$

where

$$A^i = s^2 \rho_f \hat{\phi}_v / 2s\gamma_f. \quad (10)$$

We can apply the Cagniard-de Hoop technique to the incident field (de Hoop 1960). Thus we write the pressure field in terms of the transform-domain expression of Green's function:

$$\tilde{p}^i = s^3 \rho_f \hat{\phi}_v \tilde{G}^i \quad (11)$$

where

$$\tilde{G}^i = (1/2 s^2 \gamma_f) \exp(-s\gamma_f |z - h_s|). \quad (12)$$

We transform (12) back to the space-Laplace domain with the aid of (3),

$$\hat{G}^i = \left(\frac{s}{2\pi}\right)^2 \int_{-\infty}^{+\infty} d\beta \int_{-\infty}^{+\infty} (1/2 s^2 \gamma_f) \exp\{-j\alpha x - j\beta y - s\gamma_f |z - h_s|\} d\alpha. \quad (13)$$

For the above technique we write  $\hat{G}^i$  in the form

$$\hat{G}^i = \int_{0-}^{\infty} (*) \exp(-s\tau) d\tau \quad (14)$$

by transforming the path of integration in the complex  $p$  plane such that the term in the exponent is purely real and positive:

$$\begin{cases} \text{Re}(j\alpha x + j\beta y + \gamma_f |z - h_s|) = \tau, \\ \text{Im}(j\alpha x + j\beta y + \gamma_f |z - h_s|) = 0. \end{cases} \quad (15)$$

Because  $\tau$  is purely real, we can identify it with time and we can also use Lerch's uniqueness theorem (Widder 1946) which states

if

$$\int_{0-}^{\infty} \varphi_1(t) \exp(-st) dt = \int_{0-}^{\infty} \varphi_2(t) \exp(-st) dt,$$

( $s$  is positive real and in common region of convergence)

then

$$\varphi_1(t) = \varphi_2(t).$$

Then (\*) in (14) can be recognized as the desired space-time Green's function. Thus we have evaded two integrals.

## 1.2. Description of the field quantities in the different media

In the air, the domain  $z < 0$ , the pressure is the fundamental unknown. The transform-domain representation of the transmitted field, characterized by the pressure  $\tilde{P}^a$ , is given by (for convenience)

$$\tilde{P}^a = A^a \exp(-s\gamma_f h_s + s\gamma_a z), \quad (16)$$

where

$$\gamma_a = (1/c_a^2 + \alpha^2 + \beta^2)^{1/2} \quad \text{with } \text{Re}(\gamma_a) \geq 0. \quad (17)$$

With the aid of the equation of motion, the vertical particle displacement is described by

$$\tilde{U}_z^a = -(1/s^2 \rho_a) \partial_z \tilde{P}^a. \quad (18)$$

In the fluid, the domain  $0 < z < h_w$ , the fundamental unknown is the pressure. For the pressure we can write

$$\begin{aligned} \tilde{P}^f &= \tilde{P}^i + \tilde{P}^r \\ &= A^i \exp(-s\gamma_f |z - h_s|) + A^+ \exp(-s\gamma_f z) + A^- \exp\{s\gamma_f(z - h_w)\}, \end{aligned} \quad (19)$$

where  $\gamma_f$  is defined by (8). At the boundaries we need the vertical displacement in the fluid, so we substitute (19) in the equation of motion. We arrive at

$$\tilde{U}_z^f = -(1/s^2 \rho_f) \partial_z \tilde{P}^f. \quad (20)$$

In the solid, the domain  $z > h_w$ , the wavemotion can be described by the particle displacement  $\mathbf{u}$  as the fundamental unknown quantity. The total wavemotion can be decomposed into a divergence-free part and a curl-free part, the so-called shear and compressional waves, respectively. Hence

$$\{\tilde{U}_x^t, \tilde{U}_y^t, \tilde{U}_z^t\} = \{\tilde{U}_x^s, \tilde{U}_y^s, \tilde{U}_z^s\} + \{\tilde{U}_x^p, \tilde{U}_y^p, \tilde{U}_z^p\}, \quad (21)$$

where the shear part ( $\text{div } \mathbf{u} = 0$ ) can be written (for convenience) as

$$\{\tilde{U}_x^s, \tilde{U}_y^s, \tilde{U}_z^s\} = \{\gamma_s A_x^s, \gamma_s A_y^s, -j\alpha A_x^s - j\beta A_y^s\} \exp\{-s\gamma_s(z - h_w) - s\gamma_f(h_w - h_s)\}, \quad (22)$$

with

$$\gamma_s = (1/c_s^2 + \alpha^2 + \beta^2)^{1/2} \quad \text{with } \text{Re}(\gamma_s) \geq 0 \quad (23)$$

and the compressional part ( $\text{rot } \mathbf{u} = 0$ ) as

$$\{\tilde{U}_x^p, \tilde{U}_y^p, \tilde{U}_z^p\} = \{j\alpha, j\beta, \gamma_p\} A^p \exp\{-s\gamma_p(z - h_w) - s\gamma_f(h_w - h_s)\}, \quad (24)$$

where

$$\gamma_p = (1/c_p^2 + \alpha^2 + \beta^2)^{1/2} \quad \text{with } \text{Re}(\gamma_p) \geq 0. \quad (25)$$

For the boundary conditions we need the  $xz$ ,  $yz$  and  $zz$  components of the stress tensor. They are determined by using the constitutive relation for an isotropic, perfectly elastic medium. In the transform domain these components are

$$\tilde{\tau}_{xz}^t = \mu(-j\alpha s \tilde{U}_z^t + \partial_z \tilde{U}_x^t), \quad (26)$$

$$\tilde{\tau}_{yz}^t = \mu(-j\beta s \tilde{U}_z^t + \partial_z \tilde{U}_y^t), \quad (27)$$

$$\tilde{\tau}_{zz}^t = \lambda(-j\alpha s \tilde{U}_x^t - j\beta s \tilde{U}_y^t + \partial_z \tilde{U}_z^t) + 2\mu \partial_z \tilde{U}_z^t. \quad (28)$$

### 1.3. Determination of the amplitude factors

In the description of the wavemotion in the media, we still have six unknown amplitude factors, viz.,  $A_x^s$ ,  $A_y^s$ ,  $A^p$ ,  $A^a$ ,  $A^+$  and  $A^-$ . We also have six boundary conditions so we can solve for these factors. At the air/fluid interface we require the continuity of the pressure and the continuity of the vertical displacement. Hence,

$$\lim_{z \downarrow 0} \tilde{P}^f = \lim_{z \uparrow 0} \tilde{P}^a, \quad (29)$$

$$\lim_{z \downarrow 0} \tilde{U}_z^f = \lim_{z \uparrow 0} \tilde{U}_z^a. \quad (30)$$

At a fluid/solid interface the tangential components of the traction must vanish, the normal component of the traction in the solid must be equal to the opposite of the pressure in the fluid and the normal component of the particle displacement must be continuous. Hence,

$$\lim_{z \downarrow h_w} \tilde{\tau}_{xz}^t = 0, \quad (31)$$

$$\lim_{z \downarrow h_w} \tilde{\tau}_{yz}^t = 0, \quad (32)$$

$$\begin{aligned} \lim_{z \downarrow h_w} \tilde{\tau}_{zz}^t &= \lim_{z \uparrow h_w} (-\tilde{P}^f), \\ &= -A^i \exp\{-s\gamma_f(h_w - h_s)\} - A^+ \exp(-s\gamma_f h_w) - A^-, \end{aligned} \quad (33)$$

$$\begin{aligned} \lim_{z \downarrow h_w} \tilde{U}_z^t &= \lim_{z \uparrow h_w} \tilde{U}_z^f, \\ &= -(\gamma_f/s\rho_f)[-A^i \exp\{-s\gamma_f(h_w - h_s)\} - A^+ \exp(-s\gamma_f h_w) + A^-]. \end{aligned}$$

To solve these equations, we introduce the reflection coefficients  $R_a$  and  $R_s$ :

$$A^+ = R_a [A^i \exp(-s\gamma_f h_s) + A^- \exp(-s\gamma_f h_w)], \quad (35)$$

$$A^- = R_s [A^i \exp\{-s\gamma_f(h_w - h_s)\} + A^+ \exp(-s\gamma_f h_w)]. \quad (36)$$

With the boundary conditions (31) and (32) we can express  $A_x^s$  and  $A_y^s$  in terms of  $A^p$ :

$$A_x^s = -\{j\alpha\gamma_p/(\alpha^2 + \beta^2 + 1/(2c_s^2))\}A^p, \quad (37)$$

$$A_y^s = -\{j\beta\gamma_p/(\alpha^2 + \beta^2 + 1/(2c_s^2))\}A^p. \quad (38)$$

Now we substitute these results in the boundary conditions which require the continuity of the pressure and the vertical displacement, viz., (29), (30), (33) and (34). So,

$$R_a = (\gamma_f/\rho_f - \gamma_a/\rho_a)/(\gamma_f/\rho_f + \gamma_a/\rho_a), \quad (39)$$

$$R_s = (-\rho_f\gamma_P/4\rho_s\gamma_f c_s^4 + \Delta_R)/\Delta_{sch}, \quad (40)$$

where

$$\Delta_R = (\alpha^2 + \beta^2 + 1/(2c_s^2))^2 - (\alpha^2 + \beta^2)\gamma_P\gamma_s \quad (41)$$

is the Rayleigh-wave determinant, associated with surface waves along a traction-free boundary, and

$$\Delta_{sch} = \rho_f\gamma_P/4\rho_s\gamma_f c_s^4 + \Delta_R \quad (42)$$

is the Scholte-wave determinant associated with surface waves along a fluid/solid boundary.

Now we solve for  $A^+$  and  $A^-$  with the aid of the definitions (35) and (36). We arrive at

$$A^+ = 1/(1 - R_a R_s \exp\{-2s\gamma_f h_w\})A^i \\ \times [R_a \exp(-s\gamma_f h_s) + R_a R_s \exp\{-s\gamma_f(2h_w - h_s)\}], \quad (43)$$

$$A^- = 1/(1 - R_a R_s \exp\{-2s\gamma_f h_w\})A^i \\ \times [R_a R_s \exp\{-s\gamma_f(h_w + h_s)\} + R_s \exp\{-s\gamma_f(h_w - h_s)\}]. \quad (44)$$

For the Cagniard-de Hoop technique we expand the denominator, occurring in the right-hand sides, in a power series of exponential functions. As in practical situations the recording time is finite, we observe a finite number of multiply reflected waves. The resulting expansion is convergent when  $R_a$  and  $R_s$  are real since then  $|R_a| < 1$ ,  $|R_s| < 1$  and  $|\exp(-s\gamma_f h_w)| < 1$  when  $s$  is real and positive. When we substitute these factors in the equation for the total pressure (19), we arrive at

$$\tilde{P}^i(h_r) = A^i \exp\{-s\gamma_f |z - h_s|\} \quad (45)$$

$$+ A^i \sum_{m=0}^{\infty} R_a^{m+1} R_s^m \exp[-s\gamma_f(2mh_w + h_s + h_r)] \quad (i)$$

$$+ A^i \sum_{m=0}^{\infty} R_a^{m+1} R_s^{m+1} \exp[-s\gamma_f\{2(m+1)h_w + h_r - h_s\}] \quad (ii)$$

$$+ A^i \sum_{m=0}^{\infty} R_a^m R_s^{m+1} \exp[-s\gamma_f\{2(m+1)h_w - h_s - h_r\}] \quad (iii)$$

$$+ A^i \sum_{m=0}^{\infty} R_a^{m+1} R_s^{m+1} \exp[-s\gamma_f\{2(m+1)h_w + h_s - h_r\}]. \quad (iv)$$

The latter four terms can be recognized as certain kinds of multiply reflected waves (fig. 2). From now on these reflections and the direct wave will be written symbolically as  $R_a^k R_s^l$  and the corresponding exponentials as  $\exp(-s\gamma_f D_{k,l})$ .

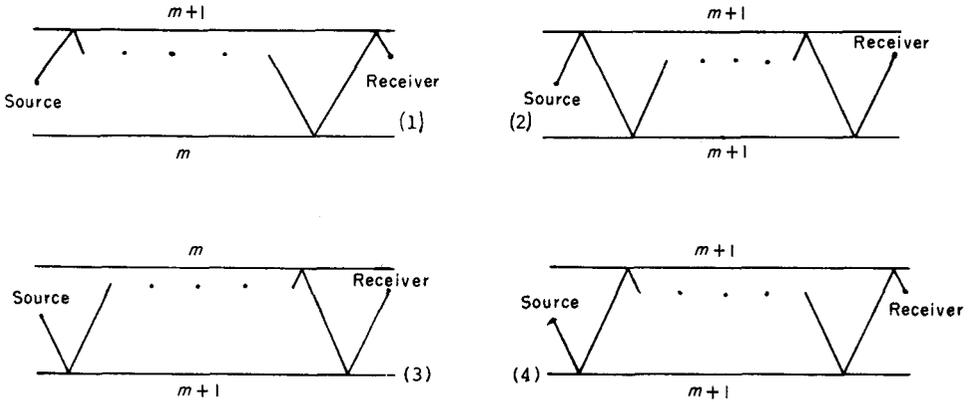


Fig. 2. The separated multiply reflected waves; the numbers refer to the terms in (45).

So far there is no special difference between the three-dimensional and the two-dimensional case because to obtain the two-dimensional from the three-dimensional case we simply omit all the  $y$ -terms or in the transform domain the  $\beta$ -terms, because  $\partial_y = 0$ . In the two-dimensional case one factor,  $s$ , has also to be dropped in the definition of Green's function. The modified Cagniard-contours for the two-dimensional and three-dimensional case are now determined separately.

1.4. Determination of Green's function for the line source problem

One element of Green's function in the  $(x, z; s)$  domain has the form

$$\hat{G}_{k,l}^r = \left(\frac{s}{2\pi}\right) \int_{-\infty}^{+\infty} (1/2s\gamma_f) R_a^k R_s^l \exp \{-s(j\alpha + \gamma_f D_{k,l})\} d\alpha. \tag{46}$$

The factors  $R_a$  and  $R_s$  in the integrand do not depend on  $s$  and therefore we can proceed with the Cagniard-de Hoop technique by substituting

$$p = j\alpha, \tag{47}$$

$$\begin{cases} (\text{Re}(p + \gamma_f D_{k,l}) = \tau & (= \text{real and positive}) \\ (\text{Im}(p + \gamma_f D_{k,l}) = 0. \end{cases} \tag{48}$$

(47) means a transformation so that the integration path is along the imaginary axis instead of the real axis. Note that  $p$  is not the pressure but an integration variable. (48) implies that the path of integration is deformed and care should therefore be taken to transform the path continuously. An extra integration should be made around any branchcut or pole that is passed (fig. 3).

Physically, the extra integrations around these branchcuts represent the so-called head waves (seismology) or lateral waves (optics) and the contribution from poles represent the surface waves. Head waves exist when the wave velocity in the second medium is larger than the velocity of the wavefront along the interface with

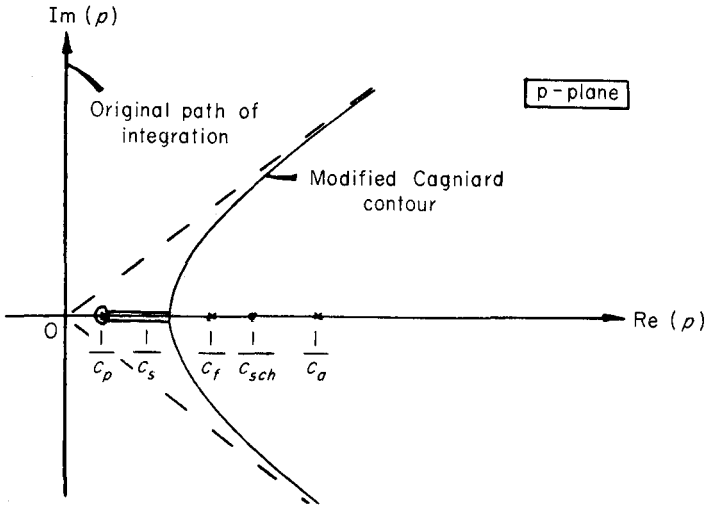


Fig. 3. The transformation in the complex  $p$ -plane according to the Cagniard-de Hoop technique.

the first medium. These waves can only be observed in certain regions in the first medium (fig. 4). The two branches of the hyperbola in the complex  $p$ -plane, representing the body waves, are supplemented by circular arcs at infinity. The contribution of this arc vanishes provided that the algebraic factors in the integrand are zero at infinity. In the case of acoustic wavefield excitation this condition will always be satisfied.

(48) implies a path in the complex  $p$ -plane that is located symmetrically with respect to the real  $p$ -axis, because Schwarz's reflection principle applies to the left-hand side.

Let  $r$  denote the horizontal distance between the source and receiver and let  $R_{k,l}$  be the total travel path, defined by

$$R_{k,l} = (r^2 + D_{k,l}^2)^{1/2}. \quad (49)$$

With Lerch's theorem the space-time Green's function can be recognized as

$$g_{k,l}^r(\tau) = \begin{cases} 0 & \text{when } -\infty < \tau < T_{fp} \\ \text{Im} \{ R_a^k R_s^l(p^{fp}) \} / 2\pi (T_{ff}^2 - \tau^2)^{1/2} & \text{when } T_{fp} < \tau < T_{ff} \\ \text{Re} \{ R_a^k R_s^l(p^{ff}) \} / 2\pi (\tau^2 - T_{ff}^2)^{1/2} & \text{when } T_{ff} < \tau < \infty; \end{cases} \quad (50)$$

where

$$T_{fp} = r/c_p + D_{k,l}(1/c_f^2 - 1/c_p^2)^{1/2} \quad (51)$$

is the arrival time of the head wave (if present),

$$T_{ff} = R_{k,l}/c_f \quad (52)$$

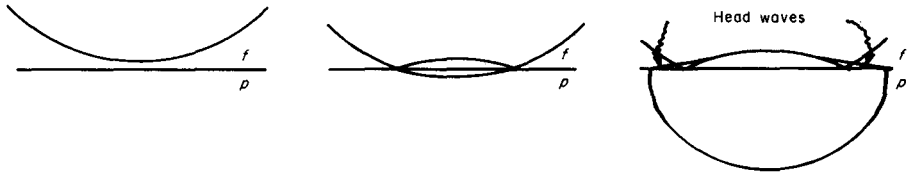


Fig. 4. The development of the wavefront in time when head waves occur. The wavespeed  $c_p$  is larger than the wavespeed of the wavefront along the interface in medium  $f$ .

is the arrival time of the body wave in the fluid and

$$p^{fp} = r/R_{k,l}^2 - D_{k,l}(R_{k,l}^2/c_f^2 - \tau^2)^{1/2}/R_{k,l}^2, \tag{53}$$

$$p^{ff} = r/R_{k,l}^2 + jD_{k,l}(\tau^2 - R_{k,l}^2/c_f^2)^{1/2}/R_{k,l}^2. \tag{54}$$

The head-wave contribution is only present in regions where  $r/R_{k,l} > c_f/c_p$ . In marine seismics this only occurs when the  $P$ -wave velocity of the material of the sea-bed is higher than the wave velocity in sea water, and the horizontal distance is large enough.

### 1.5. Determination of Green's function for the point source problem

This case is more complicated than the line source equivalent because a double integral is involved. The  $(x, y, z, s)$ -domain representation of one element of Green's function is

$$\hat{G}_{r,l}^s = \left(\frac{s}{2\pi}\right)^2 \int_{-\infty}^{\infty} d\beta \int_{-\infty}^{\infty} (1/2s^2\gamma_f) R_d^k R_s^l \exp \{-s(j\alpha x + j\beta y + \gamma_f D_{k,l})\} d\alpha. \tag{55}$$

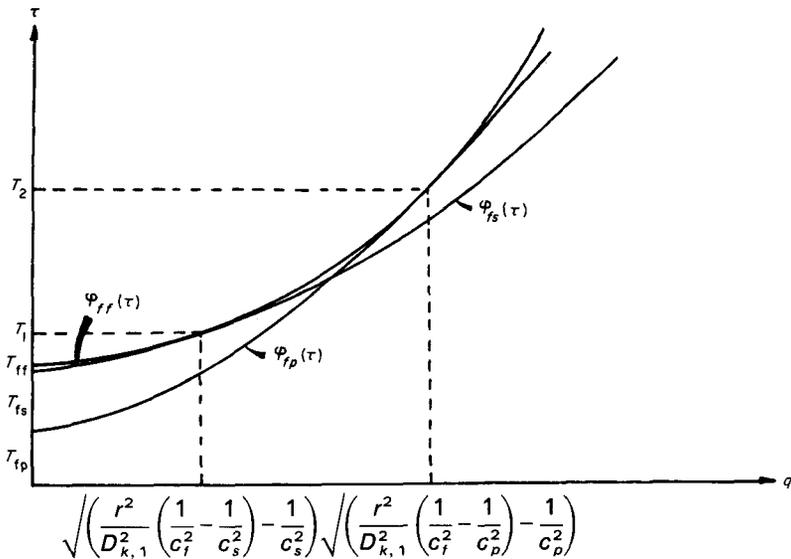


Fig. 5. Relationship between  $q$  and  $\tau$ .

As previously we follow the Cagniard-de Hoop technique but now substitute

$$\begin{aligned}\alpha &= \omega \cos(\varphi) - q \sin(\varphi), \\ \beta &= \omega \sin(\varphi) + q \cos(\varphi),\end{aligned}\tag{56}$$

where  $\varphi$  follows from the polar coordinate specification of the point of observation:  $x = r \cos(\varphi)$ ,  $y = r \sin(\varphi)$ ,

$$p = j\omega,\tag{57}$$

$$\begin{cases} \operatorname{Re}(pr + \gamma_f D_{k,l}) = \tau & (= \text{real and positive}) \\ \operatorname{Im}(pr + \gamma_f D_{k,l}) = 0.\end{cases}\tag{58}$$

Now our integrals need to be in such a form that we can use Lerch's uniqueness theorem. To change the order of integration we use the relationship between  $q$  and  $\tau$ , shown in fig. 5. The integral over  $q$  is the desired space-time Green's function:

$$g_{k,l}^r(\tau) = \begin{cases} 0 & \text{when } \infty < \tau < T_{fp} \\ \int_{0\varphi_{fp}}^{\varphi_{fp}(\tau)} \operatorname{Im} \{R_a^k R_s^l(p^{fp})\} / \{2\pi^2(T_{ff}^2(q) - \tau^2)^{1/2}\} dq & \\ & \text{when } T_{fp} < \tau < T_{ff} \\ \int_{\varphi_{ff}(\tau)}^{\varphi_{fp}(\tau)} \operatorname{Im} \{R_a^k R_s^l(p^{fp})\} / \{2\pi^2(T_{ff}^2(q) - \tau^2)^{1/2}\} dq \\ + \int_0^{\varphi_{ff}(\tau)} \operatorname{Re} \{R_a^k R_s^l(p^{ff})\} / \{2\pi^2(\tau^2 - T_{ff}^2(q))^{1/2}\} dq & \\ & \text{when } T_{ff} < \tau < T_2 \\ \int_0^{\varphi_{ff}(\tau)} \operatorname{Re} \{R_a^k R_s^l(p^{ff})\} / \{2\pi^2(\tau^2 - T_{ff}^2(q))^{1/2}\} dq & \\ & \text{when } T_2 < \tau < \infty \end{cases}\tag{59}$$

in which the limits of integration are

$$\varphi_{fp}(\tau) = [\{\tau/r - D_{k,l}(1/c_f^2 - 1/c_p^2)^{1/2}/r\}^2 - 1/c_p^2]^{1/2}\tag{60}$$

and

$$\varphi_{ff}(\tau) = (\tau^2/R_{k,l}^2 - 1/c_f^2)^{1/2},\tag{61}$$

while

$$T_{fp} = r/c_p + D_{k,l}(1/c_f^2 - 1/c_p^2)^{1/2}\tag{62}$$

is the arrival time of the head wave if present,

$$T_{ff} = R_{k,l}/c_f\tag{63}$$

is the arrival time of the body wave in the fluid and

$$T_2 = R_{k,l}^2 (1/c_f^2 - 1/c_p^2)^{1/2} / D_{k,l} \quad (64)$$

is the time after which there are no further head-wave contributions.

$$p^{fp} = r/R_{k,l}^2 - D_{k,l} (R_{k,l}^2 q^2 + R_{k,l}^2 / c_f^2 - \tau^2)^{1/2} / R_{k,l}^2. \quad (65)$$

$$p^{ff} = r/R_{k,l}^2 + jD_{k,l} (\tau^2 - R_{k,l}^2 / c_f^2 - R_{k,l}^2 q^2)^{1/2} / R_{k,l}^2. \quad (66)$$

As in the line-source case, the head-wave contribution is only present if  $r/R_{k,l} > c_f/c_p$ .

Shear head-waves can also occur with the compressional head waves that so far have only been considered. Expressions for shear head-waves are found by replacing  $c_p$  by  $c_s$  in (60), (62) and (64), which give  $\varphi_{fs}(\tau)$ ,  $T_{fs}$  and  $T_1$ , respectively. These are also drawn in fig. 5.

For numerical computation we used the transformation shown in appendix A because (inverse) square-root singularities occur at the end points of the  $q$ -integration. All the integrations are then over the interval  $(0, \pi/2)$ .

### 1.6. Numerical results for the fluid/fluid/solid configuration

We now show some numerical results following from the theory. So far, both the line source and the point source problem with only one fluid/solid boundary have been discussed extensively by de Hoop and van der Hijden (1983, 1984). The computer program to evaluate Green's function has been developed independently of these authors and we compared their program and ours. We chose the input parameters to reproduce the figures presented by de Hoop and van der Hijden. Agreement up to three significant digits was achieved. The differences originated from the time values at which the Green's function was evaluated, and from different evaluations of the integral(s).

In all figures, the total Green's function was evaluated to include the direct wave. The travel path of the direct wave is denoted by  $R_{0,0}$  and its arrival time by  $T_f$ .

First, we discuss the *two-dimensional* case. In the numerical evaluation of Green's function every multiply reflected wave is treated separately because the modified-Cagniard contour differs for each one. For every multiply reflected wave we have another vertical travel path  $D_{k,l}$ , so different expressions for  $p^{ff}$  and  $p^{fp}$  arise.

We discuss a few figures for the two-dimensional case. There is a disadvantage in the two-dimensional case: for every multiply reflected wave Green's function has a discontinuity at time  $t = T_{ff}$ , so it often shows a bigger value for a multiply reflected wave than the direct wave. But the two-dimensional case requires relatively little computation time.

In fig. 6, we chose the rounded-off values derived from a borehole log for the velocities. In this case we are in the region where we have no contributions from head waves. Head waves occur only when the horizontal distance from source to receiver is larger than 208 m. The offset in fig. 6a is 180 m which is not very large in comparison with the water depth, 100 m. The direct wave arrives at  $t = 0.12$  s and

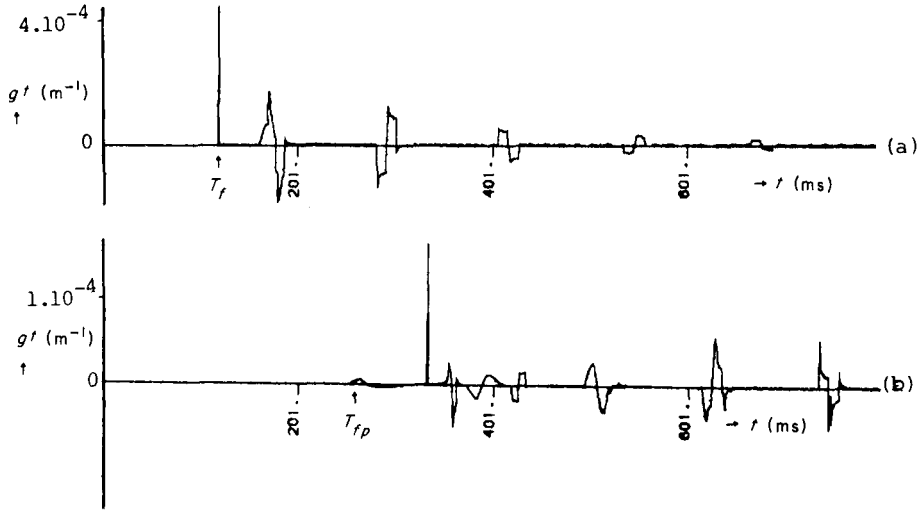


Fig. 6. Two-dimensional space-time Green's function with:  $c_a = 334$  m/s,  $c_p = 2000$  m/s,  $c_f = 1500$  m/s,  $c_s = 600$  m/s,  $\rho_a/\rho_f = 0.0013$ ,  $\rho_s/\rho_f = 2.5$ ,  $h_s = 9$  m,  $h_r = 7.5$  m,  $h_w = 100$  m; (a)  $r = 180$  m and (b)  $r = 500$  m.

then a few milliseconds later the ghost reflection of the source. Neither arrival is disturbed by any head-wave contributions. However, when the offset is larger, fig. 6b, head-wave contributions are present in the first reflections.

In fig. 7a, the case of a solid with high wavespeeds is shown. Head waves are abundantly present even with a small offset. When the receiver is located farther

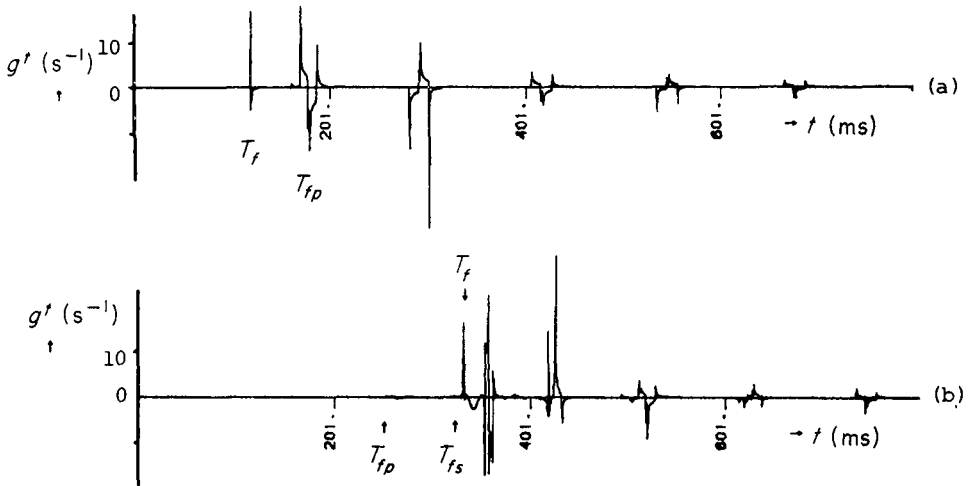


Fig. 7. Two-dimensional space-time Green's function with:  $c_a = 334$  m/s,  $c_f = 1500$  m/s,  $c_s = 2000$  m/s,  $c_p = 3500$  m/s,  $\rho_a/\rho_f = 0.0013$ ,  $\rho_s/\rho_f = 2.5$ ,  $h_s = 9$  m,  $h_r = 7.5$  m,  $h_w = 100$  m; (a)  $r = 180$  m and (b)  $r = 500$  m.

Table 2. *The five relevant intervals when compressional and shear head-wave contributions occur.*

$\tau$ interval	$q$ interval
$T_{fp} < \tau < T_{fs}$	$0 < q < \varphi_{fp}$
$T_{fs} < \tau < T_{ff}$	$0 < q < \varphi_{fs}, \quad \varphi_{fs} < q < \varphi_{fp}$
$T_{ff} < \tau < T_1$	$0 < q < \varphi_{ff}, \quad \varphi_{ff} < q < \varphi_{fs}, \quad 0 < q < \varphi_{fp}$
$T_1 < \tau < T_2$	$0 < q < \varphi_{ff}, \quad \varphi_{ff} < q < \varphi_{fp}$
$T_2 < \tau < \infty$	$0 < q < \varphi_{ff}$

away from the source, fig. 10, the first arrival is a compressional head wave but shear head waves also arrive at the receiver before the direct wave. These first arrivals are used in refraction seismics. A shear head wave arriving before the body wave occurs when the shear-wave velocity is larger than the compressional-wave velocity in the fluid. Even in high-order, multiply reflected waves, head-wave contributions are visible. Note that in figs 6 and 7 there are times when the Green's function has a larger amplitude for a multiply reflected wave than the direct wave because of the inverse square-root singularity for each multiply reflected wave.

To compute Green's function with the contribution of 24 multiply reflected waves on a Gould 32/67 computer takes about 1 minute, for 1 s recording time, with a sampling interval of 0.5 ms.

We now discuss the *point source* problem. In the integrand (inverse) square-root singularities occur at the end points of the integration interval. With the aid of the transformation shown in appendix A these disappear. When the shear-wave velocity is larger than the fluid-wave velocity, the integrand shows a discontinuity in slope at

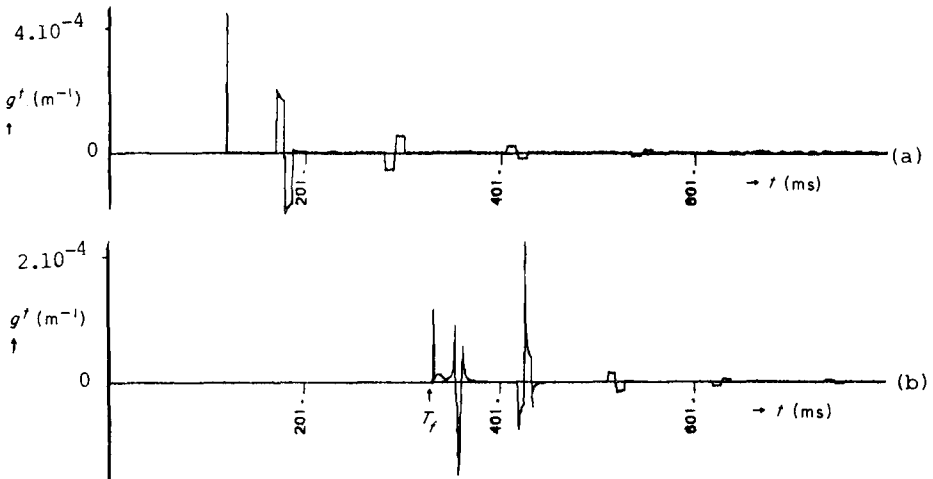


Fig. 8. Three-dimensional space-time Green's function with:  $c_a = 334$  m/s,  $c_f = 1500$  m/s,  $c_p = 2000$  m/s,  $c_s = 600$  m/s,  $\rho_a/\rho_f = 0.0013$ ,  $\rho_s/\rho_f = 2.5$ ,  $h_s = 9$  m,  $h_r = 7.5$  m,  $h_w = 100$  m; (a)  $r = 180$  m and (b)  $r = 500$  m.

time  $t = T_{fs}$ . This is why we decompose the relevant integral into three integrals over the intervals  $T_{fs} < \tau < T_{ff}$ ,  $T_{ff} < \tau < T_1$  and  $T_1 < \tau < T_2$  as long as shear head-wave contributions occur. This means that the evaluation of Green's function consists of five relevant intervals, given in table 2. In fig. 8 the values are the same as for fig. 6, except that the source is a point instead of a line. The first part of the trace to 320 ms is enlarged in fig. 9a and is decomposed into all its components as shown in figs 9b-f. Figure 9b shows the direct wave, which has an amplitude of  $1/4\pi R_{0,0}$  and is time-shifted from the origin by an amount of  $R_{0,0}/c_f$ . This is the well-known monopole solution of the wave equation for an infinite homogeneous medium. In fig. 9c the ghost reflection of the source arrives just after the direct wave but with a smaller amplitude because of the angle-dependent reflection coefficient  $R_a$ . This figure corresponds to the multiply reflected wave (45.i). Figures 9d-f are the multiply reflected waves (45.ii)-(45.iv).

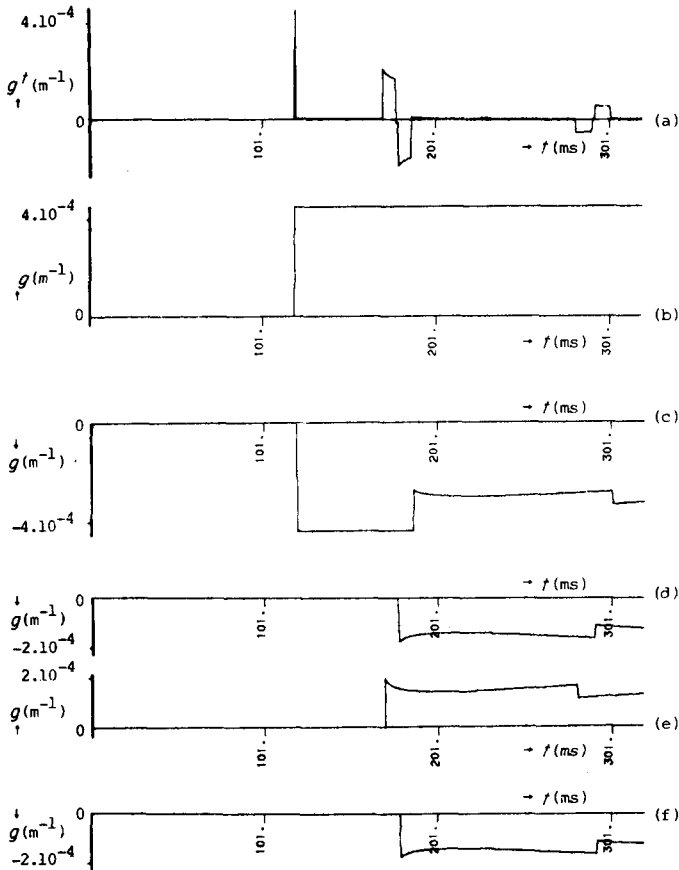


Fig. 9. The first 320 ms of fig. 8a decomposed into its components, according to (45): (a) the first 320 ms, (b) the direct wave, (c) multiple 1, (d) multiple 2, (e) multiple 3 and (f) multiple 4.

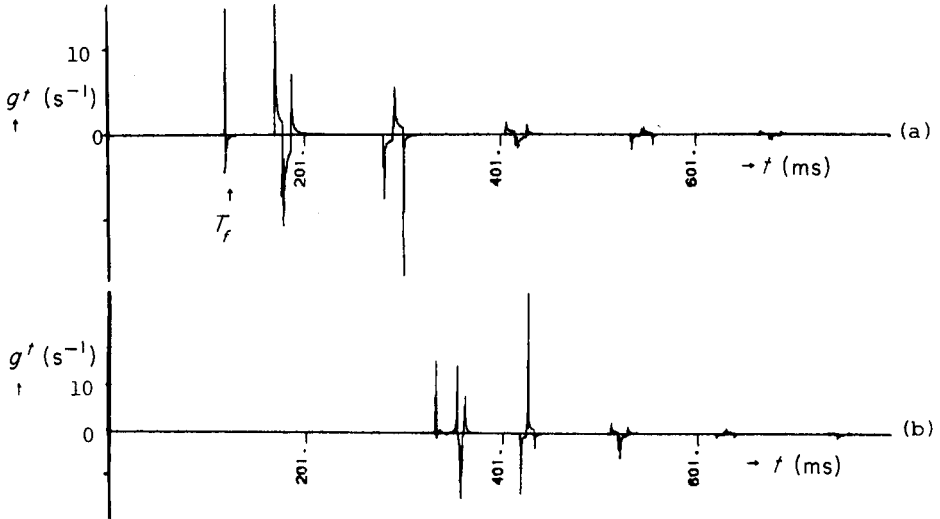


Fig. 10. Three-dimensional space-time Green's function with:  $c_a = 334$  m/s,  $c_f = 1500$  m/s,  $c_p = 3500$  m/s,  $c_s = 1400$  m/s,  $\rho_a/\rho_f = 0.0013$ ,  $\rho_s/\rho_f = 2.5$ ,  $h_s = 9$  m,  $h_r = 7.5$  m,  $h_w = 100$  m; (a)  $r = 180$  m and (b)  $r = 500$  m.

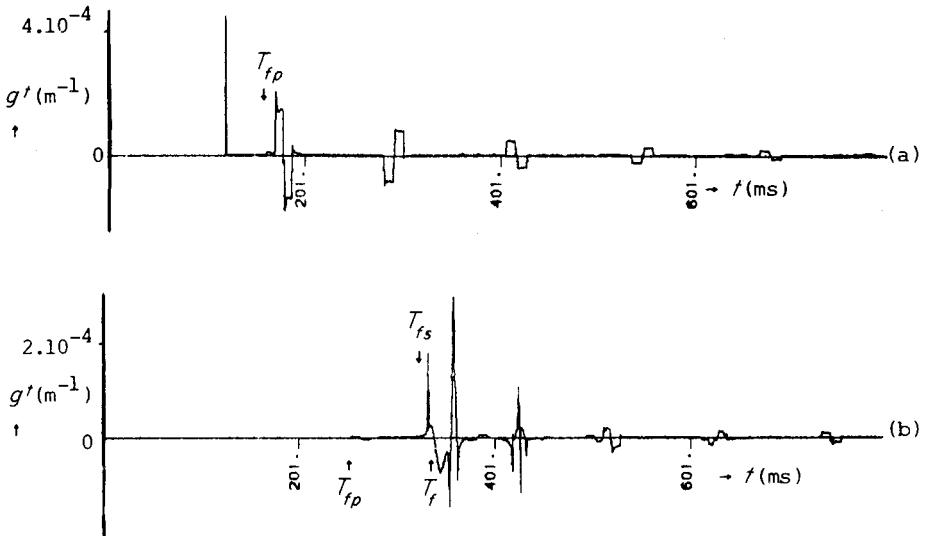


Fig. 11. Three-dimensional space-time Green's function with:  $c_a = 334$  m/s,  $c_f = 1500$  m/s,  $c_p = 3500$  m/s,  $c_s = 2000$  m/s,  $\rho_a/\rho_f = 0.0013$ ,  $\rho_s/\rho_f = 2.5$ ,  $h_s = 9$  m,  $h_r = 7.5$  m,  $h_w = 100$  m; (a)  $r = 180$  m and (b)  $r = 500$  m.

Figure 8b shows the response with the same input parameters and the offset increased to 500 m.

In fig. 10 onwards the compressional-wave velocity is increased. Figure 10 shows the response for shear-wave velocity still lower than the fluid-wave velocity. An increase in offset for this configuration causes more compressional head waves to be present (fig. 10b). For fig. 11 both the compressional and the shear-wave velocity are larger than the fluid-wave velocity. The first 450 ms are very complicated so again the components are separated (figs. 12a-f). The direct wave arrives at  $t = 0.33$  s and then the ghost reflection given in fig. 12c. Figures 12d-f are the reflections as given in (45). An increase in offset only makes the recognition of the different arrivals more difficult (see fig. 11b).

To compute Green's function for one of these figures with the contributions of 30 multiply reflected waves takes about 30 minutes on a Gould 32/67 computer.

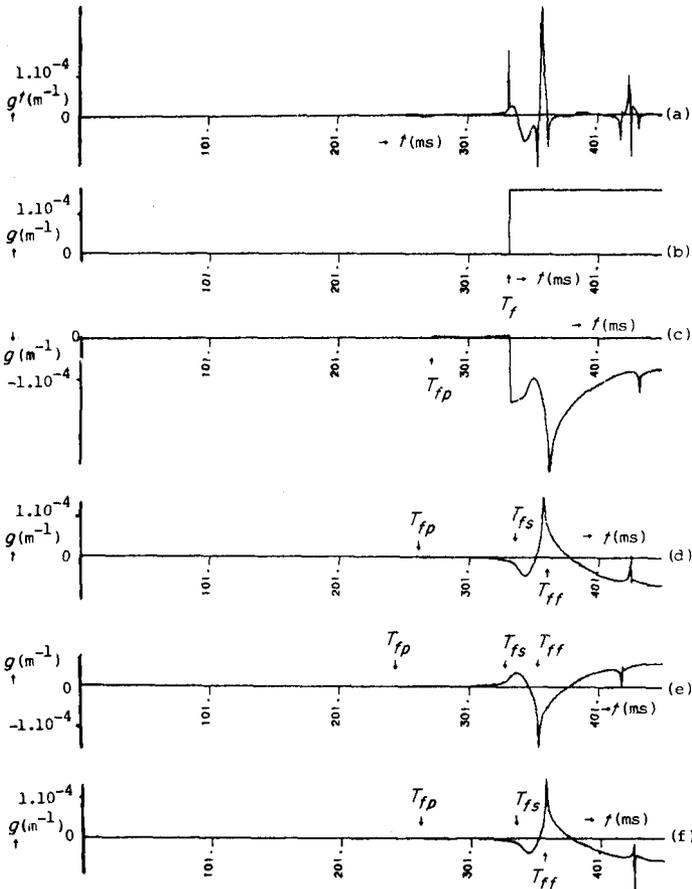


Fig. 12. The first 450 ms of fig. 11b decomposed into its components, according to (45): (a) the first 450 ms, (b) the direct wave, (c) multiple 1, (d) multiple 2, (e) multiple 3 and (f) multiple 4.

### 1.7. Convolution

To make a synthetic seismogram, a convolution of the three-dimensional Green's function with a source signature is performed. A source signature from a source modeling program (Metselaar 1984) simulates the signature of an airgun with a chamber volume of 0.98 l (= 60 cu inch) and firing pressure of  $1.379 \cdot 10^7$  Pa (= 2000 psi). This source signature, is such that convolution with Green's function, apart from a factor, gives what would be measured in practice. The signature, shown in fig. 13a, is the pressure as a function of time, but what we want is an expression in terms of  $\varphi_v$ . (9) gives the solution for the incident field. In order to gather information about the system we write, for the reflected acoustic pressure—in accordance with the three-dimensional Green's function (55)—

$$\hat{P}^r = s^3 \rho_f \hat{\varphi}_v \hat{G}^r. \quad (67)$$

The same kind of expression was derived in the general framework for the incident field, but now Green's function looks more complicated because of the large number of reflections. We want to write this equation with  $\hat{p}^i$  instead of  $\hat{\varphi}_v$ . Thus we transform (9) back to the space-Laplace domain analytically with the aid of the Cagniard-de Hoop technique (de Hoop 1960):

$$\hat{P}^i = (s^2 \rho_f \hat{\varphi}_v / 4\pi R_{0,0}) \exp(-sR_{0,0}/c_f). \quad (68)$$

The term  $s^3 \rho_f \hat{\varphi}_v$  in front of Green's function in (67) can now be written as

$$s^3 \rho_f \hat{\varphi}_v = 4\pi R_{0,0} s \hat{p}^i \exp(sR_{0,0}/c_f). \quad (69)$$

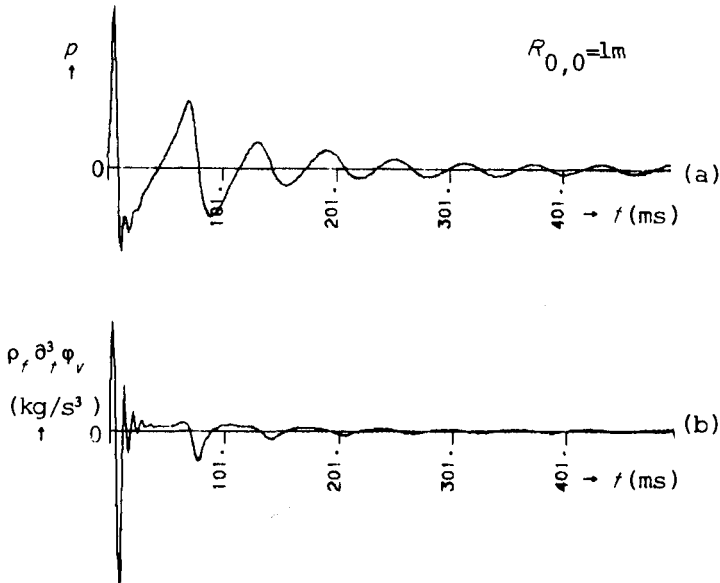


Fig. 13. (a) The simulated airgun signature as a function of time and (b) its term  $\rho_f \partial_t^3 \varphi_v$ .

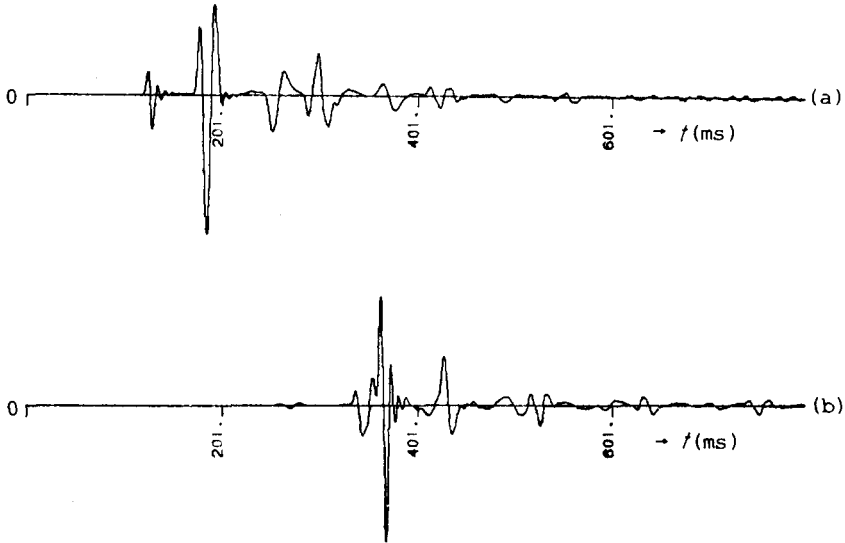


Fig. 14. The convolution of term  $\rho_f \partial_t^3 \varphi_v$  for the simulated airgun signature with Green's function as in fig. 8a for (a), while for (b) Green's function as in fig. 11b has been taken.

This term is reproduced in the space-time domain in fig. 13b. Because the pressure is measured at 1 m distance from the source,  $R_{0,0} = 1$  m. The multiplication can be performed in the Laplace domain and  $\hat{p}^i$  can be transformed back to the space-time domain. This has been done in fig. 14: in (a) convolution was performed with fig. 8a, while in (b) fig. 11a was taken as input function.

## PART 2. STACK OF FLUID LAYERS WITH THE SOURCE AND RECEIVER IN THE UPPER HALF-SPACE

### 2.1. The solution in the transform domain

We now consider a stack of acoustic layers between two elastic half-spaces. The source and receiver are situated in the upper half-space, fig. 15. The origin of the right-handed Cartesian coordinate system is chosen in the upper half-space with the  $z$  axis pointing downwards and the source starting at  $t = +0$ .  $h_s$  is the source depth and  $h_r$  the receiver depth, the depth of the  $n$ th interface is  $h_n$ ;  $h_0$  applies to the receiver or source depth. The total number of layers is  $N$ , which includes the two half-spaces. We only calculate the primary reflections (and head wave, if present), so no internal multiply reflected waves are involved. The properties of the media are characterized by

$$c_n = (K_n/\rho_n)^{1/2} \quad n = 1, 2 \dots N, \quad (70)$$

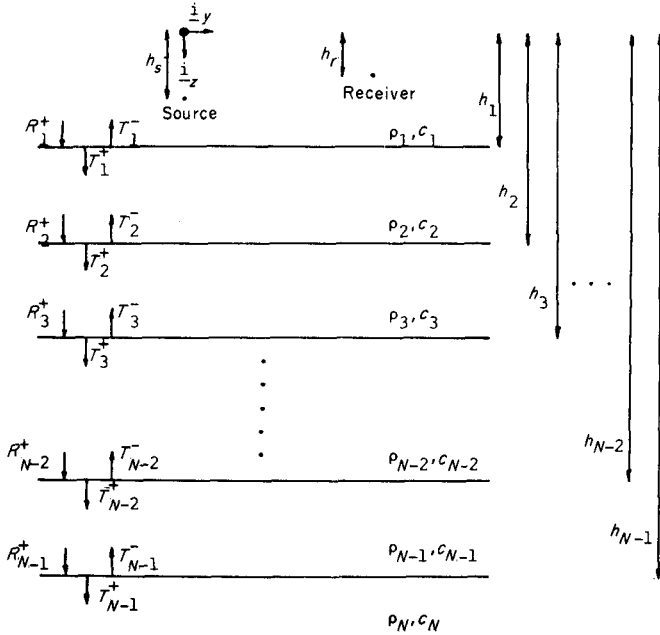


Fig. 15. The second configuration to be considered:  $N$  fluid layers.

where  $K_n$  is the bulk modulus of compression,  $\rho_n$  the volume density of mass and  $c_n$  the wave speed. The total pressure in each medium is written as

$$\tilde{P}_n^t = A_n^+ \exp \{-s\gamma_n(z - h_{n-1})\} + A_n^- \exp \{-s\gamma_n(h_n - z)\} \quad n = 1, 2 \dots N, \quad (71)$$

where

$$A_N^- = 0 \quad (72)$$

and

$$A_1^+ = A^i. \quad (73)$$

The factors  $A_n^+$  and  $A_n^-$  denote downgoing and upgoing waves, respectively. To solve for  $A_n^+$  and  $A_n^-$ , we apply the boundary conditions at each interface where we require the continuity of the pressure and the continuity of the vertical displacement. Hence,

$$\lim_{z \downarrow h_n} \tilde{P}_{n+1}^t = \lim_{z \uparrow h_n} \tilde{P}_n^t \quad n = 1, 2 \dots N - 1, \quad (74)$$

$$\lim_{z \downarrow h_n} \tilde{U}_{z, n+1}^t = \lim_{z \uparrow h_n} \tilde{U}_{z, n}^t \quad n = 1, 2 \dots N - 1. \quad (75)$$

We introduce the reflection coefficients  $R_n^+$  and transmission coefficients  $T_n^-$  and  $T_n^+$  through

$$A_n^+ = T_{n-1}^+ A_{n-1}^+ \exp \{-s\gamma_{n-1}(h_{n-1} - h_{n-2})\} \quad n = 2 \dots N, \quad (76)$$

$$A_n^- = R_n^+ A_n^+ \exp \{-s\gamma_n(h_n - h_{n-1})\} + T_n^- A_{n+1}^- \exp \{-s\gamma_{n+1}(h_{n+1} - h_n)\} \\ n = 1 \dots N - 1. \quad (77)$$

The coefficients  $R_n^+$  and  $T_n^+$  are found by substituting these equations in the boundary conditions (74) and (75), while the coefficient  $T_n^-$  is found by placing the source in the lower half-space. Note that no reflection coefficient for reflection against the lower side of an interface is present, because we consider only primary reflections. We arrive at

$$R_n^+ = (\gamma_n/\rho_n - \gamma_{n+1}/\rho_{n+1})/(\gamma_n/\rho_n + \gamma_{n+1}/\rho_{n+1}), \quad (78)$$

$$T_n^+ = 2(\gamma_n/\rho_n)/(\gamma_n/\rho_n + \gamma_{n+1}/\rho_{n+1}) \quad (79)$$

and

$$T_n^- = 2(\gamma_{n+1}/\rho_{n+1})/(\gamma_n/\rho_n + \gamma_{n+1}/\rho_{n+1}). \quad (80)$$

We now determine the space-time Green's function for the two-dimensional and the three-dimensional case. Therefore we write the reflections symbolically as  $T_{n-1}R_n$ , where

$$T_{n-1} = \prod_{k=1}^{n-1} T_k^+ T_k^-. \quad (81)$$

## 2.2. Green's function for the line source problem

Now we must transform the solution back to the space-Laplace domain. The same kind of expression as (46) results, only the reflection factors and the exponential differ. As in part 1, we substitute  $p = j\alpha$  and require the exponential to be of the form  $\exp(-st)$ . Thus

$$\operatorname{Re} \left\{ j\alpha r + 2 \sum_{k=1}^n \gamma_k (h_k - h_{k-1}) \right\} = \tau, \\ \operatorname{Im} \left\{ j\alpha r + 2 \sum_{k=1}^n \gamma_k (h_k - h_{k-1}) \right\} = 0. \quad (82)$$

Except from the first reflection, all contributions from other reflections contain more than one propagation coefficient in the exponential, so in those cases a simple analytical expression for the modified Cagniard contour does not exist. The contour can be calculated with the aid of a numerical technique (de Hoop 1979) given in appendix B.

With our substitutions, for one contribution of Green's function in the space-time domain we arrive at

$$g_n^r(\tau) = \begin{cases} 0 & \text{when } -\infty < \tau < T^{HW} \\ \frac{1}{2\pi} \operatorname{Im} \{T_{n-1} R_n \partial_\tau p^{HW} / 2\gamma_1\} & \text{when } T^{HW} < \tau < T^{BW}, \\ \frac{1}{2\pi} \operatorname{Im} \{T_{n-1} R_n \partial_\tau p^{BW} / 2\gamma_1\} & \text{when } T^{BW} < \tau < \infty \end{cases} \quad (83)$$

where

$$T^{HW} = r/c_{n+1} + 2 \sum_{k=1}^n (1/c_k^2 - 1/c_{n+1}^2)^{1/2} (h_k - h_{k-1}) \quad (84)$$

is the arrival time of the head wave (if present), while

$$T^{BW} = 2 \sum_{k=1}^n (h_k - h_{k-1}) / (c_k \cos \theta_k) \quad (85)$$

is the arrival time of the body wave. This value is found by determining the point of intersection of the contour with the real  $p$ -axis, where the minimum value of  $t$  leads to an infinitely large value of  $\partial_\tau p^{BW}$ . This is accomplished by a numerical technique (appendix B).

### 2.3. Green's function for the point source problem

In the three-dimensional case, an expression equivalent to (55) results. To determine our space-time Green's function, we follow the procedure of the Cagniard-de Hoop technique. We follow the steps for the three-dimensional case in part 1 by introducing polar coordinates, integrating along the imaginary  $p$ -axis instead of along the real  $p$ -axis, requiring the exponential to take the form  $\exp(-st)$  and finally, interchanging the order of integration. One element of Green's function is represented in the space-time domain by

$$g_n^r(\tau) = \begin{cases} 0 & \text{when } -\infty < \tau < T^{HW} \\ \frac{1}{2\pi^2} \int_0^{q^{HW}(\tau)} \operatorname{Im} \{T_{n-1} R_n \partial_\tau p^{HW} / 2\gamma_1\} dq & \text{when } T^{HW} < \tau < T^{BW} \\ \frac{1}{2\pi^2} \int_{q^{BW}(\tau)}^{q^{HW}(\tau)} \operatorname{Im} \{T_{n-1} R_n \partial_\tau p^{HW} / 2\gamma_1\} dq \\ \quad + \frac{1}{2\pi^2} \int_0^{q^{BW}(\tau)} \operatorname{Im} \{T_{n-1} R_n \partial_\tau p^{BW} / 2\gamma_1\} dq & \text{when } T^{BW} < \tau < T_M \\ \frac{1}{2\pi^2} \int_0^{q^{BW}(\tau)} \operatorname{Im} \{T_{n-1} R_n \partial_\tau p^{BW} / 2\gamma_1\} dq & \text{when } T_M < \tau < \infty \end{cases} \quad (86)$$

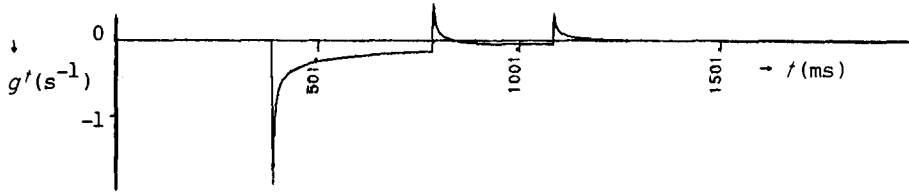


Fig. 16. Two-dimensional space-time Green's function for the case of four layers with only primary reflections. Further,  $c_1 = 1500$  m/s,  $c_2 = 3000$  m/s,  $c_3 = 5000$  m/s,  $c_4 = 9000$  m/s,  $\rho_1 = 1010$  kg/m<sup>3</sup>,  $\rho_2 = 200$  kg/m<sup>3</sup>,  $\rho_3 = 400$  kg/m<sup>3</sup>,  $\rho_4 = 2000$  kg/m<sup>3</sup>,  $h_s = 9$  m,  $h_r = 7.5$  m,  $h_1 = 300$  m,  $h_2 = 900$  m,  $h_3 = 1650$  m,  $r = 50$  m.

when the limit of integration  $q^{BW}(t)$  follows from  $T^{BW}(q)$  as expressed in (B7). The time  $T^{HW}$ , the arrival time of the head wave, is given by (84), while the time  $T^{BW}$ , the arrival time of the body wave, is given by (85). The time  $T_M$ ,

$$T_M = \sum_{k=1}^n (1/c_k^2 - 1/c_{n+1}^2)^{1/2} (h_k - h_{k-1}) + r \tan(\theta_1) (1/c_1^2 - 1/c_{n+1}^2)^{1/2}, \quad (87)$$

is the time beyond which head-wave contributions no longer occur.

#### 2.4. Numerical results for a stack of fluid layers

The results from this configuration approximate a practical case of exploration seismology. The wavespeeds derived from a borehole log can now be used to calculate the forward problem. The assumptions are still restricting, i.e., homogeneous plane fluid layers, but the results are accurate.

In figs 16 and 17 we have used a model of four layers, so there are three reflecting interfaces. The two-dimensional case is shown in fig. 16, the three-dimensional case in fig. 17. For clarity, we have decomposed Green's function into its components (figs 17b-d). To show a seismic trace, we have convolved this Green's function with a synthetic source signature, as found in fig. 18a. The result of the convolution and the factor  $\rho_f \partial_t^3 \varphi_v$ , for this signature is given in fig. 18b. The result of the convolution of this function leads to fig. 19.

Another two-dimensional case is shown in fig. 20, where nine layers are involved. Figure 21 shows the corresponding three-dimensional one. Again, we have convolved this function with the synthetic function, fig. 18. The result is shown in fig. 22.

With this technique we can concentrate on only an interesting part of the seismic section or some important reflecting interfaces, but still take into account the wave propagation in the upper layers. This considerably lowers the computation time.

To compute Green's function for a nine-layer case on a Gould 32/67 computer takes about 2 minutes for the two-dimensional case and for the three-dimensional case about 30 minutes.

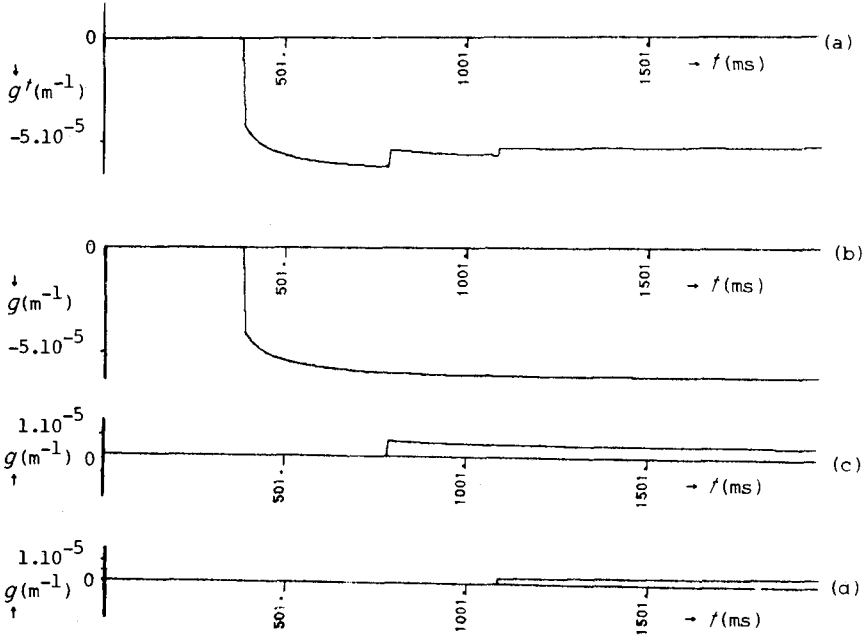


Fig. 17. Three-dimensional space-time Green's function for the case of four layers with only primary reflections. (a) shows the total function, which is decomposed into its components in (b)–(d). Further,  $c_1 = 1500$  m/s,  $c_2 = 3000$  m/s,  $c_3 = 5000$  m/s,  $c_4 = 9000$  m/s,  $\rho_1 = 1010$  kg/m<sup>3</sup>,  $\rho_2 = 200$  kg/m<sup>3</sup>,  $\rho_3 = 400$  kg/m<sup>3</sup>,  $\rho_4 = 2000$  kg/m<sup>3</sup>,  $h_s = 9$  m,  $h_r = 7.5$  m,  $h_1 = 300$  m,  $h_2 = 900$  m,  $h_3 = 1650$  m,  $r = 50$  m.

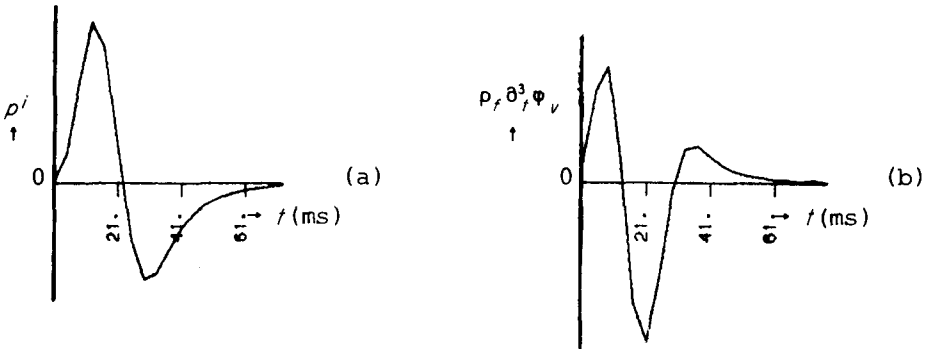


Fig. 18. The synthetic source signature with the pressure as a function of time (a), and its derived function  $\rho_f \partial_t^3 \phi_v$  (b).

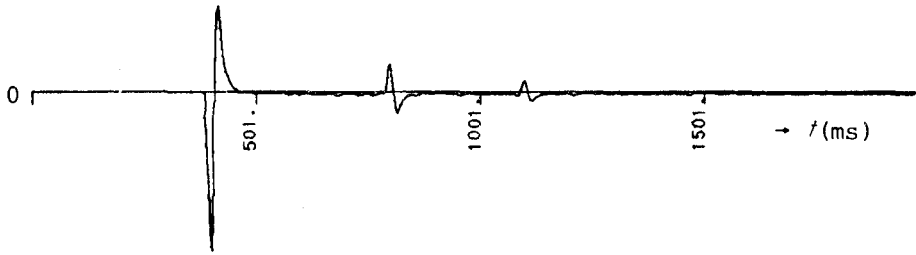


Fig. 19. The convolution of the four-layer case as in fig. 17a, with the synthetic function, as in fig. 18b.

### 3. CONCLUSIONS

With the aid of the Cagniard-de Hoop technique a simple closed-form expression is derived for the acoustic pressure in the fluid in space-time when an air/fluid/solid configuration or a stack of fluid layers is excited by an impulsive monopole source. A straightforward expression arises in the two-dimensional configuration (line source problem) and a single bounded integral in the three-dimensional case (point source problem) have to be evaluated. Reflected and refracted waves have been illustrated by numerical results. In contrast to the standard time-space Fourier and Fourier-Bessel inversion integrals, our expressions do not show any oscillatory behaviour, and computation times are much lower. In the case of fluid layers, the computation times are longer, but the method remains very accurate. Therefore, the Cagniard-de Hoop technique is recommended as a check on approximate methods for the same problem or for inverse modeling pertaining to these configurations.

### ACKNOWLEDGMENTS

We thank Royal Dutch Shell for financial aid which enabled us to finish this investigation, to present part 1 at the 47th EAEG meeting in Budapest and to prepare this publication. We would also like to thank Sietse de Vries, affiliate of Professor de Hoop in the Electronics Department of Delft University of Technology, for his program which calculates numerically the modified Cagniard

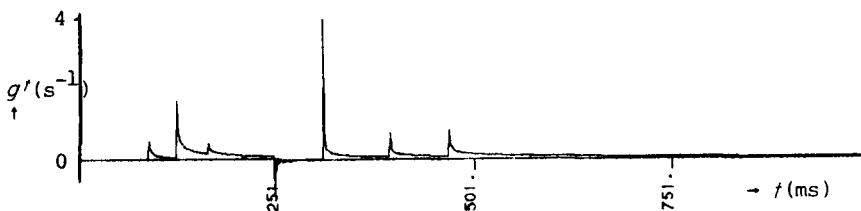


Fig. 20. Two-dimensional space-time Green's function for the case of nine layers with only primary reflections. The wave speeds, densities and depths are given in table 3, while  $h_s = 9$  m,  $h_r = 7$  m and  $r = 50$  m.

Table 3. *The depths, densities and wave velocities for the nine-layer case.*

Layer no.	$h_n$ (m)	$\rho_n$ (kg/m <sup>3</sup> )	$c_n$ (m/s <sup>2</sup> )
1	70	1000	1500
2	100	1010	1600
3	135	1200	1700
4	175	1200	1800
5	210	1250	1700
6	260	1150	1600
7	340	1200	1900
8	415	1300	2000
9	$\infty$	1500	2200

contour. Finally, thanks to discussions with René du Cloux and Professor Ziolkowski, both of Delft University of Technology, many improvements were made.

#### APPENDIX A

The integrals in the three-dimensional case, as in (55), are of the general form

$$I = \int_{\varphi_1(t)}^{\varphi_2(t)} \text{Int}(q) dq. \quad (\text{A1})$$

In the evaluation, problems arise at the end points of the integration due to (inverse) square-root singularities. These problems are avoided by changing the variable of integration through

$$q^2 = \varphi_1^2(t) \cos^2(\psi) + \varphi_2^2(t) \sin^2(\psi). \quad (\text{A2})$$

Then the interval of integration is mapped on to the fixed interval  $(0, \pi/2)$ , while

$$dq = \{\varphi_2^2(t) - \varphi_1^2(t)\} \cos(\psi) \sin(\psi) / \{\varphi_1^2(t) \cos^2(\psi) + \varphi_2^2(t) \sin^2(\psi)\}^{1/2} d\psi. \quad (\text{A3})$$

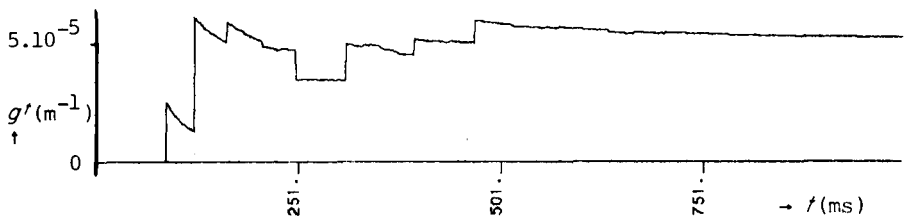


Fig. 21. Three-dimensional space-time Green's function for the case of nine layers with only primary reflections. The wave speeds, densities and depths are given in table 3, while  $h_s = 9$  m,  $h_r = 7$  m and  $r = 50$  m.

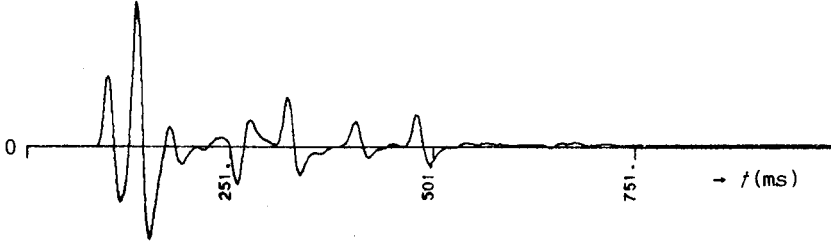


Fig. 22. The convolution of the nine-layer case as in fig. 21, with the synthetic function as in fig. 18b.

### APPENDIX B

We show how to determine a modified Cagniard contour when more than one propagation coefficient is involved. We follow the procedure given by de Hoop (1979) for a  $n$ -layer case extended to the three-dimensional case by de Vries (1984). The requirement for the modified Cagniard contour for  $n$  layers is

$$\begin{aligned} \operatorname{Re} \left( pr + \sum_{n=1}^N \gamma_n d_n \right) &= \tau \quad (\text{is purely real and positive}), \\ \operatorname{Im} \left( pr + \sum_{n=1}^N \gamma_n d_n \right) &= 0, \end{aligned} \quad (\text{B1})$$

where  $d_n = h_n - h_{n-1}$  is the vertical distance through layer  $n$ . Consider the part of the Cagniard contour which tends to infinity, corresponding to a body wave. Let

$$p = p^{BW}(t) \quad \text{with } T^{BW} \leq t < \infty \quad (\text{B2})$$

represent the body wave in the first quadrant of the complex  $p$ -plane. Because Schwarz's reflection principle applies to the left-hand side of (B1), we can say that if  $p^{BW}(t)$  is a solution  $p^{BW*}(t)$  is also a solution (\* denotes complex conjugate).  $T^{BW}$  in (B2) denotes the arrival time. This value is reached at the point of intersection of (B2) with the real  $p$ -axis, where the minimum of  $t$  leads to an infinitely large value of  $\partial_\tau p^{BW}$ . By differentiating (B1) with respect to  $t$ , we get

$$\partial_\tau p^{BW} = \left[ r - \sum_{n=1}^N (p^{BW}/\gamma_n) d_n \right]^{-1}. \quad (\text{B3})$$

Let  $\theta_1 \dots \theta_N$  be angles that are mutually related through Snell's law of refraction; then

$$p = \theta_1 \sin(\theta_1) = \theta_2 \sin(\theta_2) = \dots = \theta_N \sin(\theta_N) \quad (\text{B4})$$

makes the denominator of the right-hand side of (B3) vanish provided that

$$r - \sum_{n=1}^N d_n \tan(\theta_n) = 0. \quad (\text{B5})$$

Substitution of (B4) in (B1) yields

$$T^{BW}(q) = \sum_{n=1}^N \frac{d_n \theta_n}{\cos(\theta_n)}, \quad (\text{B6})$$

which is the total travelttime for a disturbance to propagate from the source to the point of observation along a trajectory that is in accordance with Fermat's principle.

So far only the body-wave arrivals are considered. It is possible that a propagation coefficient is involved in the reflection/transmission coefficients which is not present in (B1), because  $d_n$  is zero. When the branchcut due to this propagation coefficient is less than the intersection point of the contour  $p = p^{BW}$  with the real  $p$ -axis, then an additional loop integral along the branchcut must be included. This part of the modified Cagniard contour corresponds to a head wave. Let

$$p = p^{HW}(t) \quad \text{with } T^{HW} \leq \tau < T^{BW} \quad (\text{B7})$$

denote its parametric representation in the first quadrant of the complex  $p$  plane, then the head-wave part of the modified Cagniard contour consists of  $p = p^{HW}$  and  $p = p^{HW*}$ .

The calculations must be determined with the aid of a numerical technique when  $N$  is larger than one. A numerical technique of an iterative nature can be speeded up by choosing the starting value judiciously. Therefore, the values  $p = P^{BW}$  and  $p = P^{HW}$  obtained from

$$pr + (\Omega^2 - p^2)^{1/2} D = \tau, \quad (\text{B8})$$

where  $D$  and  $\Omega$  are chosen such that (B7) approximates (B1), are suitable. In (B8) we select the values of  $D$  and  $\Omega$  so that (B8) coincides with (B1) as  $|p| \rightarrow \infty$  and at  $p = 0$ . From

$$P^{BW} \simeq \tau \left/ \left( r - \gamma \sum_{n=1}^N d_n \right) \right., \quad \text{as } \tau \rightarrow \infty \quad (\text{B9})$$

and

$$P^{BW} \simeq \tau / (r - jH), \quad \text{as } \tau \rightarrow \infty \quad (\text{B10})$$

it follows that

$$D = \sum_{n=1}^N d_n, \quad (\text{B11})$$

while the conditions,

$$P^{BW} = 0 \quad \text{at } \tau = \sum_{n=1}^N \Omega_n d_n \quad (\text{B12})$$

and

$$P^{BW} = 0 \quad \text{at } \tau = \Omega D \quad (\text{B13})$$

lead to

$$\Omega = \frac{\sum_{n=1}^N \Omega_n d_n}{\sum_{n=1}^N d_n}. \quad (\text{B14})$$

In these equations  $\Omega_n = (1/c_n^2 + q^2)^{1/2}$  is real and positive. Solving (B7) and (B8), the starting value  $P^{BW}$  of  $p^{BW}$  in the iteration process is then given by

$$P^{BW} = \tau r / (r^2 + D^2) + jD \{ \tau^2 - (r^2 + D^2) \Omega^2 \}^{1/2} / (r^2 + D^2), \quad (\text{B15})$$

when

$$(r^2 + D^2)^{1/2} \Omega < \tau < \infty,$$

and the starting value  $P^{HW}$  of  $p^{HW}$  by

$$P^{HW} = \tau r / (r^2 + D^2) - D \{ (r^2 + D^2) \Omega^2 - \tau^2 \}^{1/2} / (r^2 + D^2), \quad (\text{B16})$$

when

$$D\Omega < \tau < (r^2 + D^2)^{1/2} \Omega. \quad (\text{B17})$$

Note that in the two-dimensional case,  $\Omega_n$  is simply  $1/c_n$ .

## REFERENCES

- AKI, K. and RICHARDS, P.G. 1980, Body waves in media with depth-dependent properties, *in* Quantitative Seismology I, chapter 9, W.H. Freeman.
- CAGNIARD, L. 1939, Réflexion et réfraction des ondes sismiques progressives, Gauthiers-Villars.
- CAGNIARD, L. 1962, Reflexion and Refraction of Progressive Seismic Waves, translated from French by E.A. Flinn and C.H. Dix, McGraw-Hill.
- HELMBERGER, D.V. 1968, Appendix to The crust-mantle transition in the Bering Sea, *Bulletin of the Seismological Society of America* 58, 179–214.
- HOOP, A.T. DE, 1960, A modification of Cagniard's method for solving seismic pulse problems, *Applied Scientific Research, Section B8*, 349–356.
- HOOP, A.T. DE, 1979, Pulsed electromagnetic radiation from a line source in a two-media configuration, *Radio Science* 14(2), 253–268.
- HOOP, A.T. DE and HIJDEN, J.H.M.T. VAN DER, 1983, Generation of acoustic waves by an impulsive line source in a fluid/solid configuration with a plane boundary, *Journal of the Acoustical Society of America* 74, 333–342.
- HOOP, A.T. DE and HIJDEN, J.H.M.T. VAN DER, 1984, Generation of acoustic waves by an impulsive point source in a fluid/solid configuration with a plane boundary, *Journal of the Acoustical Society of America* 75, 1709–1715.
- METSelaar, G. 1984, The Pressure Field of an Airgun Array (unpublished), M.Sc. thesis, Delft University of Technology.
- VRIES, S.M. DE, 1984, On the computation of modified Cagniard contours, PA 4320, PA 4630M, PA 9130, Electronics Department, Delft University of Technology.
- WIDDER, D.V. 1946, *The Laplace Transform*, Princeton University Press.